






## Physical Processes Determine Spatial Structure in Water Temperature and Residence Time on a Wide Reef Flat

 E. C. Reid<sup>1</sup> , S. J. Lentz<sup>2</sup> , T. M. DeCarlo<sup>2,3</sup> , A. L. Cohen<sup>2</sup> , and K. A. Davis<sup>1,4</sup> 

<sup>1</sup>Department of Civil and Environmental Engineering, University of California, Irvine, CA, USA, <sup>2</sup>Department of Geology and Geophysics, Woods Hole Oceanographic Institution, Woods Hole, MA, USA, <sup>3</sup>Now at Hawai'i Pacific University, Honolulu, HI, USA, <sup>4</sup>Department of Earth System Science, University of California, Irvine, CA, USA

### Key Points:

- On a coral atoll, thermal microclimates exist, with gradients in mean temperature and daily temperature range from the reef crest to lagoon
- Wind, waves, and tides are all significant forces driving flow on the reef flat
- Reefs that are wide compared to tidal excursion length may exhibit complex spatial patterns in residence time and thermal microclimates

### Correspondence to:

K. A. Davis,  
[davis@uci.edu](mailto:davis@uci.edu)

### Citation:

Reid, E. C., Lentz, S. J., DeCarlo, T. M., Cohen, A. L., & Davis, K. A. (2020). Physical processes determine spatial structure in water temperature and residence time on a wide reef flat. *Journal of Geophysical Research: Oceans*, 125, e2020JC016543. <https://doi.org/10.1029/2020JC016543>

Received 29 JUN 2020  
 Accepted 19 NOV 2020

**Abstract** On coral reefs, flow determines residence time of water influencing physical and chemical environments and creating observable microclimates within the reef structure. Understanding the physical mechanisms driving environmental variability on shallow reefs, which distinguishes them from the open ocean, is important for understanding what contributes to thermal resilience of coral communities and predicting their response to future anomalies. In June 2014, a field experiment conducted at Dongsha Atoll in the northern South China Sea investigated the physical forces that drive flow over a broad shallow reef flat. Instrumentation included current and pressure sensors and a distributed temperature sensing system, which resolved spatially and temporally continuous temperature measurements over a 3-km cross-reef section from the lagoon to reef crest. Spectral analysis shows that while diurnal variability was significant across the reef flat—a result expected from daily solar heating—temperature also varied at higher frequencies near the reef crest. These spatially variable temperature regimes, or thermal microclimates, are influenced by circulation on the wide reef flat, with spatially and temporally variable contributions from tides, wind, and waves. Through particle tracking simulations, we find the residence time of water is shorter near the reef crest (3.6 h) than near the lagoon (8.6 h). Tidal variability in flow direction on the reef flat leads to patterns in residence time that are different than what would be predicted from unidirectional flow. Circulation on the reef also determines the source (originating from offshore vs. the lagoon) of the water present on the reef flat.

**Plain Language Summary** Ocean warming due to climate change threatens coral reefs worldwide. However, corals that live in naturally variable thermal environments have been shown to be more resilient to bleaching. Understanding the processes that drive flow on a coral reef, including wind, waves and tides, can determine how long offshore water spends on the shallow reef, and thus water temperature and the rate of chemical and biological processes on the reef. In this study, we show that on a wide reef flat at Dongsha Atoll in the northern South China Sea, the way water moves and the amount of time it spends in different regions can vary substantially. This leads to spatial patterns in average water temperature and in the daily range of temperature that corals experience across the reef. Understanding which corals live in more naturally variable regions, and as a result may be more resilient in a changing climate, is important for prioritizing protection and mitigation.

## 1. Introduction

Coral reefs are increasingly threatened by rising seawater temperatures, and the collapse of reefs on a global scale has been predicted to occur in the near future (Donner, 2009; Hoegh-Guldberg et al., 2007; Van Hooidonk et al., 2016). Understanding the variation in environmental conditions over small spatial and temporal scales has become increasingly important when considering the variation in the physiological responses of coral colonies within a reef to stressors (DeCarlo, Cohen, Wong, Davis, et al., 2017; Guadayol et al., 2014; McClanahan et al., 2005; Oliver & Palumbi, 2011; Pandolfi et al., 2011; Riegl & Piller, 2003; van Woesik et al., 2012). Since patterns of spatial variability on a reef scale (<750 m) are not available globally with current satellite products, many studies have focused on in situ observations of temperature variability across a reef (DeCarlo, Cohen, Wong, Davis, et al., 2017; Guadayol et al., 2014; Leichter et al., 2006; Pineda et al., 2013; van Woesik et al., 2012). Recent evidence suggests that resilience to thermal stress may be influenced by a coral's thermal history, particularly at diurnal and semidiurnal time scales (DeCarlo, Cohen, Wong, Davis, et al., 2017; Castillo et al., 2012; Guadayol et al., 2014; Oliver & Palumbi, 2011; Rogers

et al., 2016; Safaie et al., 2018). The shallow depths of reef structures lead to high spatial and temporal variability in the physical environment (e.g., temperature and flow), distinguishing the reef environment from the surrounding open ocean. It is this variability that influences coral community structure and may promote resilience to thermal stress (Safaie et al., 2018), and likely other stressors (e.g., acidification, Barkley et al., 2015; Shamberger et al., 2014). Understanding the physical mechanisms underpinning this variability is important for not only recognizing resilience potential, but also predicting how reef conditions will be modified by a changing climate.

Thermal and chemical environments on coral reefs are shaped by circulation. The processes that drive flow on coral reefs range from large spatial scales, such as tides, down to small spatial scales, such as turbulence within a coral canopy (Lowe & Falter, 2015; Monismith, 2007). The major physical processes driving circulation on most shallow coral reef systems are tides, waves, and wind, and the contribution of each mechanism can vary (Lowe & Falter, 2015). For deeper reefs, ocean currents and internal waves can be important, too (Davis et al., 2008, 2020; Lowe & Falter, 2015; Schramek et al., 2018).

As surface waves break on coral reef crests, radiation stresses cause a setup of the sea surface height at the reef crest. A pressure gradient is developed that forces flow across the reef. Surface gravity waves dominate circulation on many shallow coral reef systems, and for this reason, many studies have focused on understanding this forcing (Gourlay & Colleter, 2005; Hearn, 1999; Hench et al., 2008; Kraines et al., 1998; Lowe et al., 2005, 2009a, 2009b; Symonds et al., 1995; Taebi et al., 2011).

The role of wind and tidal forcing varies across coral reefs globally. Wind-driven flow has been found to be relatively minor compared to wave- and tidally driven circulation on many reef flats (Hench et al., 2008; Rogers et al., 2016; Taebi et al., 2011). While some reefs do not experience significant tides (Hench et al., 2008), tidal forcing can be a dominant process driving flow on other reefs (Rogers et al., 2016; Taebi et al., 2011), especially when tidal ranges >3 m (Lowe & Falter, 2015). Tides can also modulate where waves break (Becker et al., 2014; Taebi et al., 2011). In some cases, tides control flow in areas such as the lagoon or channels, but not on the reef flat (Lowe et al., 2009b).

Dongsha Atoll is a vibrant coral reef and Taiwanese National Park located in the northern South China Sea (SCS; Figures 1a and 1b). Previous work has shown that cold and nutrient-rich water is regularly injected onto the shallow east reef flat, from large shoaling internal waves (Davis et al., 2020; Fu et al., 2012; Reid et al., 2019; Wang et al., 2007). Here, we examine the processes that drive flow on the east reef flat of Dongsha Atoll and characterize the resulting benthic thermal environments using a Distributed Temperature Sensing (DTS) system, which resolves spatially continuous temperature measurements along a fiber optic cable (Hausner et al., 2011; Reid et al., 2019; Selker et al., 2006; Sinnett et al., 2020; Tyler et al., 2009).

## 2. Materials and Methods

### 2.1. Site Description

Dongsha Atoll is 28 km in diameter and has an area of approximately 600 km<sup>2</sup> (Dai, 2004). The east reef flat, which is the focus of this study (Figure 1c), is roughly 3 km wide, and water depth at mean sea level ranges from 0.3 to 4.0 m (Shih et al., 2011), with shallower depths toward the reef crest. The tidal range on the reef flat is approximately 0.9 m. The forereef has a 4% slope down to 25 m depth, beyond which it steepens to 15% to 50 m depth, after which it flattens slightly to 7% to 300 m depth. A survey of the benthic composition of the reef flat shows the region is dominated by fleshy algae, sea grass, and live coral (DeCarlo, Cohen, Wong, Shiah, et al., 2017). The reef slope has a spur and groove formation, which is primarily soft corals.

General ocean circulation in the northern SCS during the summer is controlled by monsoon winds (Hu et al., 2000). Wind from the southwest drives surface currents generally to the northeast (Morton & Blackmore, 2001). Internal waves generated in the Luzon Strait (between Taiwan and the Philippines) travel westward toward Dongsha Atoll, where they become highly nonlinear bores and boluses in shallow waters (<30 m), and transport subthermocline (cold and nutrient rich) water into the nearshore region (Alford et al., 2015; Davis et al., 2020; Fu et al., 2012). Internal waves and locally generated internal tides change the stratification offshore, and can modify sea level at the reef crest, which may contribute to driving flow across

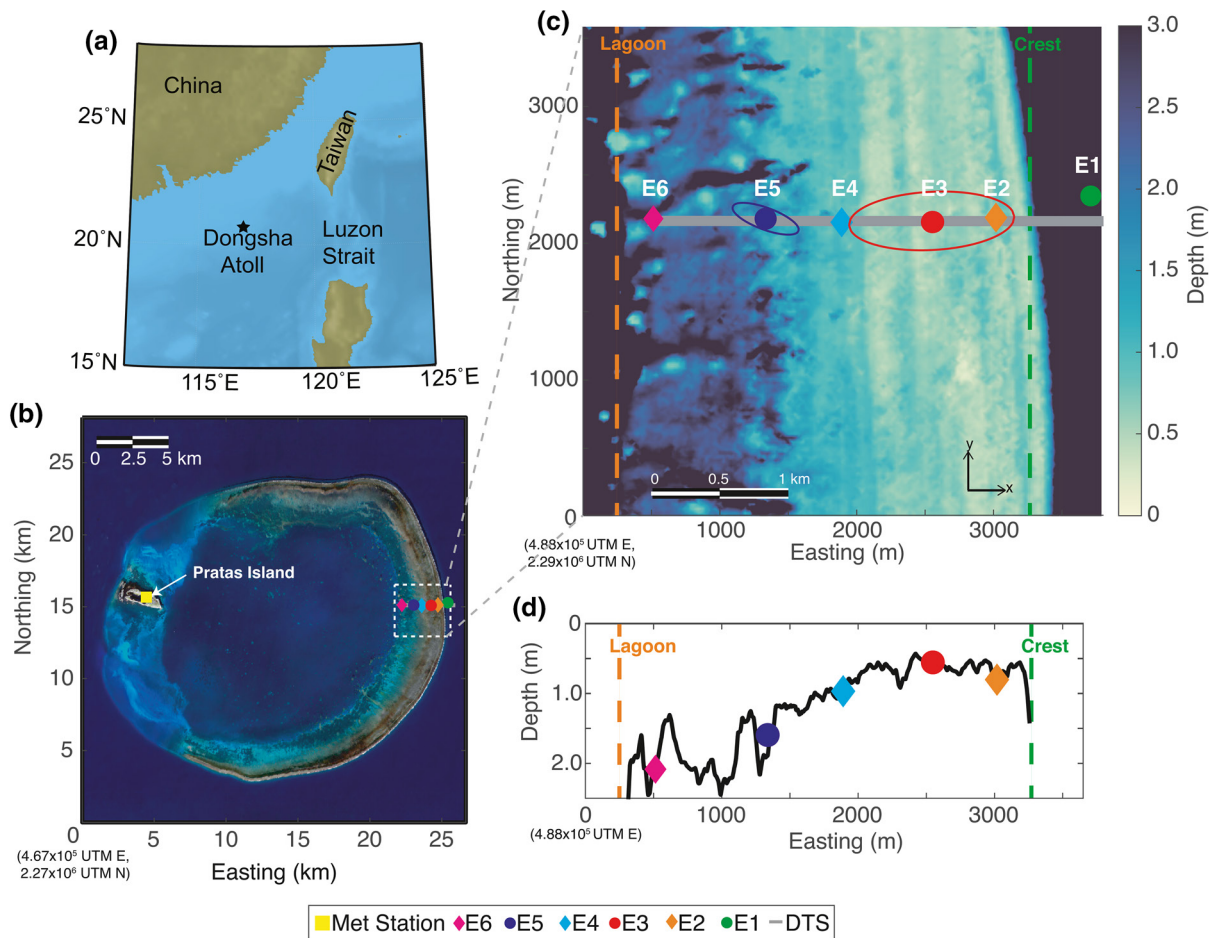


**Figure 1.** Oceanographic setting of Dongsha Atoll. Panel (a) Location of Dongsha Atoll within the northern South China Sea and Panel (b) Satellite image of Dongsha Atoll from the Taiwan National Space Organization. White box indicates region covered by Panel (c). The meteorological station located on Pratas Island is shown with a yellow square marker. Panel (c) East reef flat of Dongsha Atoll, where moorings E1 to E6 are shown. Bathymetry from LIDAR data is shown (Shih et al., 2011). The locations of Seagauge pressure sensors are shown with diamonds (E2, E4, and E6), and Aquadopp current meters (E3 and E5) and AWAC current meter (E1) are shown with circles. The location of the DTS cable is shown as a gray line. Ellipses of the principal axes of the depth-averaged currents at E3 and E5 are shown at their respective locations on the reef. The reef flat boundaries, used in particle tracking (Section 2.4), are shown with orange (lagoon) and green (reef crest) dashed lines. Panel (d) Cross section of the LIDAR bathymetry of the reef flat where the DTS was located, and moorings E2 to E6. AWAC, Acoustic Wave and Current Profiler; DTS, Distributed Temperature Sensing; LIDAR, Light Detection and Ranging.

the reef (see Section 4.1). This water is subsequently transported onto the shallow reef flat by tides, wind, and surface waves, where it alters the thermal and chemical environment (Reid et al., 2019).

## 2.2. Experiment

The observations presented here are part of a larger study of coral ecology, reef-scale circulation, and internal wave dynamics at Dongsha Atoll (see Davis et al., 2020; DeCarlo, Cohen, Wong, Davis, et al., 2017; DeCarlo, Cohen, Wong, Shiah, et al., 2017; Reid et al., 2019). In this study, we focus on measurements of currents, pressure, and water temperature taken on the reef flat on the east side of the atoll and meteorological conditions measured on Pratas Island (Figures 1b and 1c), collected from 4 to 17 June 2014. This study took place during the summer monsoon season in the SCS.

Two 2-MHz Nortek AquaDopp Profilers were placed on the reef flat at E3 and E5 (Figure 1c) to measure currents and pressure at 4-min intervals. The depth at E3 and E5 was on average 0.4 and 1.5 m, respectively. At times, water depth at E3 was too shallow for the AquaDopp to accurately measure currents. Gaps in velocity data were interpolated if the gap was less than 6 h. When water depth was less than 0.25 m, velocity data are not shown or used in this study.

An upward-looking Acoustic Wave and Current Profiler (AWAC, Nortek AS) was deployed at 18.1 m depth at E1 on the forereef (Figures 1b and 1c), and recorded current measurements at 1-min intervals and measured surface wave statistics in 20-min bursts every 3 h. Current measurements from E1 were not used in this study; however, for reference they can be found in Figure 2 of Reid et al. (2019).

Three Seabird Electronics Seagauges (SBE-26) were placed on the reef flat at E2, E4, and E6 (Figure 1c) to measure pressure at 10-min intervals. Water depths at E2, E4, and E6 were on average 0.6, 0.9, and 2.0 m, respectively.

The meteorological data used in this study were measured from the weather station located on Pratas Island (Figure 1b). The station carries sensor suites for measuring wind speed and direction.

Raman spectra fiber-optic DTS technology was deployed at Dongsha Atoll from 4 to 11 June 2014 to measure near bed water temperatures across the east reef flat and forereef slope over a 4-km distance. A Sentinel Oryx DTS interrogator collected continuous independent temperature measurements every 2 m along a Kaiphone (flexible white, 6 mm, and steel-reinforced) fiber optic cable at a sample frequency of one temperature trace per minute.

The fiber optic cable was deployed on the bottom in the cross-shelf direction on the east reef flat starting near the lagoon and going east across the reef flat and down the reef slope to a depth of approximately 50 m (Figure 1b). For the purposes of this study, we will focus on the temperature measurements taken from a 3-km section of the cable deployed on the reef flat. The DTS measurements started on June 4, 2014, and continued until the machine lost power due to Tropical Storm Hagibis on June 12, 2014. Details of deployment and calibration are found in Reid et al. (2019). The average bias and root-mean-square difference between the validation loggers (SBE-56s) and the DTS was  $0.07 \pm 0.01^\circ\text{C}$  and  $0.20 \pm 0.02^\circ\text{C}$ , respectively.

Section 3.2 Spectral analysis of DTS temperature data across the reef flat was completed using the multi-taper method (Lilly, 2019; Thomson, 1982). The 95% confidence interval is found from the  $\chi_k^2$  distribution with the six degrees of freedom given by orthogonal Slepian tapers (Thomson, 1982).

Tidal velocities offshore of the reef crest (near E1) were estimated using the Oregon State Tidal Inversion Software (Egbert & Erofeeva, 2002) and the Tide Model Driver (TMD) toolbox (Padman & Erofeeva, 2004).

### 2.3. Estimating Tide, Wave, and Wind-Driven Flow

An analysis of the currents on the Dongsha reef flat at E3 and E5 was performed to determine the physical processes that govern flow, following Lentz et al. (2016). Assuming steady-state flow and neglecting along-shore variations (i.e., that along-reef variations in bathymetry are negligible, and waves break uniformly along the length of the reef) continuity in depth-averaged flow implies that cross-reef transport,  $q_0(t)$ , does not vary across the reef (Lentz et al., 2016).

$$U(\eta + \eta_0 + h) = U(\eta + D) = q_0 \quad (1)$$

where  $U(x,t)$  is the depth-averaged cross-reef current including the Stokes velocity due to waves,  $\eta(x,t)$  is the sea level variation over the scale of the reef due to wave forcing (wave setup),  $\eta_0$  is the sea level variation on spatial scales that are large compared to the reef, which include tides, wind forcing, and seasonal buoyancy forcing,  $h(x)$  is the water depth relative to mean sea level when currents are weak, and  $D(x,t) = \eta_0(t) + h(x)$ . Based on our observations, we know that  $\eta \ll D$ , so that  $\eta + D \approx D$ , as variations in  $\eta$  are typically centimeters and  $D$  is about 1 m.

The steady, depth-averaged cross-reef momentum balance becomes:

$$\frac{\partial(U^2 D)}{\partial x} = -gD \frac{\partial \eta}{\partial x} - \frac{1}{\rho} \frac{\partial S_{xx}}{\partial x} + \frac{\tau^{sx}}{\rho} - \frac{\tau^{bx}}{\rho} \quad (2)$$

where  $g = 9.81 \text{ m s}^{-2}$  is the gravitational acceleration,  $S_{xx}$  is the cross-reef component of the wave-radiation stress tensor, in  $\text{kg s}^{-2}$ ,  $\rho$  is the density of seawater, in  $\text{kg m}^{-3}$ ,  $\tau^{sx}$  is the wind stress, and  $\tau^{bx}$  is the bottom stress, in Pa (Lowe et al., 2009b; Mei, 1989). The wave-radiation stress tensor,  $S_{xx}$  is estimated as follows:

$$S_{xx} = \frac{\rho g H_s^2}{16} \left\{ (\cos^2(\theta_w) + 1) \frac{c_g}{c} - \frac{1}{2} \right\} \quad (3)$$

where  $H_s$  is the significant wave height, in m, measured at E2, E4, and E6, and  $\theta_w$  is the wave direction,  $c_g$  is the group velocity, and  $c$  is the phase velocity (Longuet-Higgins & Stewart, 1962, 1964). Bottom stress is estimated as:

$$\tau^{bx} = \rho C_{da} U |U| = \rho C_{da} \frac{q_0 |q_0|}{D^2} \quad (4)$$

where  $C_{da}(x,t)$  is a bulk drag coefficient for the depth-averaged current (Rosman & Hench, 2011). The depth-dependence of drag has been shown to be important on coral reefs (Lentz et al., 2017) and is estimated as follows:

$$C_{da} = \kappa^2 \left\{ \log \left( \frac{D}{z_0} \right) + (\Pi - 1) \right\}^{-2} \quad (5)$$

where  $\kappa = 0.4$  is the von Karman constant,  $z_0$  is the hydrodynamic roughness, and  $\Pi$  is the Coles wake strength, which is taken as 0.2. Hydrodynamic roughness,  $z_0$ , was estimated for the Dongsha Atoll reef flat in a previous study by Lentz et al. (2017), as 3.2 cm for E3 and 1.4 cm for E5 (Figure 1c). Dividing Equation 2 by  $D$  and using Equation 1 yields:

$$-\frac{q_0^2}{D^3} \frac{\partial D}{\partial x} = -g \frac{\partial \eta}{\partial x} - \frac{1}{\rho D} \frac{\partial S_{xx}}{\partial x} + \frac{\tau^{sx}}{\rho D} - C_{da} \frac{q_0 q_0}{D^3} \quad (6)$$

Integrating Equation 6 from  $x_1$  to  $x_2$  to estimate the sea level difference  $\Delta\eta = \eta(x_2) - \eta(x_1)$ :

$$g\Delta\eta = -q_0 |q_0| \left( \int_{x_1}^{x_2} C_{da} D^{-3} dx + \frac{1}{2} \text{sgn}(q_0) D^{-2} \Big|_{x_1}^{x_2} \right) + \int_{x_1}^{x_2} \left( -\frac{1}{\rho D} \frac{\partial S_{xx}}{\partial x} + \frac{\tau^{sx}}{\rho D} \right) dx \quad (7)$$

Solving for  $q_0$  yields:

$$q_0 |q_0| = \left( \int_{x_1}^{x_2} \left( -\frac{1}{\rho D} \frac{\partial S_{xx}}{\partial x} + \frac{\tau^{sx}}{\rho D} \right) dx - g\Delta\eta \right) / \left( \int_{x_1}^{x_2} C_{da} D^{-3} dx + \frac{1}{2} \text{sgn}(q_0) D^{-2} \Big|_{x_1}^{x_2} \right) \quad (8)$$

Similar to Lentz et al. (2016), Equation 8 can be simplified by recognizing that the bathymetric slope on the reef flat is very small (i.e., the magnitude of  $dD/dx$  is negligible). Equation 8 reduces to:

$$U |U| = -\frac{\Delta S_{xx}}{\rho C_{da} \Delta x} + \frac{\tau^{sx}}{\rho C_{da}} - \frac{g\Delta\eta D}{C_{da} \Delta x} \quad (9)$$

$$U = \text{sgn} \left( -\frac{\Delta S_{xx}}{\rho C_{da} \Delta x} + \frac{\tau^{sx}}{\rho C_{da}} - \frac{g\Delta\eta D}{C_{da} \Delta x} \right) \sqrt{\left| -\frac{\Delta S_{xx}}{\rho C_{da} \Delta x} + \frac{\tau^{sx}}{\rho C_{da}} - \frac{g\Delta\eta D}{C_{da} \Delta x} \right|} \quad (10)$$

where  $\Delta x = x_2 - x_1$ . For E3,  $x_1$  and  $x_2$  are E4 and E2, and for E5, they are E6 and E4, respectively.

Equation 10 states that for a two-dimensional control volume over the reef, the on-reef flux of momentum due to the incident wave radiation stress, wind stress and pressure gradient is balanced by the bottom stress. Equation 10 was used to estimate flow due to surface waves, wind, and pressure gradients across the reef using 3 h low pass filtered observations of water depth, wind speed and direction, and wave parameters. Results are not sensitive to filter cutoff periods between 1 and 6 h.

The last term on the right-hand side of Equation 9 captures pressure gradients on the reef flat due to tides, wind, and offshore surface waves. A unified tidal analysis and prediction method (Codiga, 2011) was used to



find the tidally driven component of the sea level change ( $\Delta\eta_{\text{tide}}$ ). Offshore waves that break on the reef crest (between E1 and E2) also create a pressure gradient which drives flow across the reef. The tidal residual of the pressure gradient term ( $\Delta\eta_r = \Delta\eta - \Delta\eta_{\text{tide}}$ ) is assumed to be driven by the wave setup, but could also have some influence of tides and wind, which is discussed in Section 4.1. Wave energy that is not dissipated at the reef crest and is transmitted onto the reef flat contributes to the  $\Delta S_{xx}$  term in Equation 10. Equation 9 can be reorganized to account for the two pressure gradient terms ( $\Delta\eta_{\text{tide}}$  and  $\Delta\eta_r$ ).

$$U|U| = -\frac{\Delta S_{xx}}{\rho C_{da} \Delta x} + \frac{\tau^{sx}}{\rho C_{da}} - \frac{g \Delta \eta_{\text{tide}} D}{C_{da} \Delta x} - \frac{g \Delta \eta_r D}{C_{da} \Delta x} \quad (11)$$

The first and the fourth term in Equation 11 represent the flow driven by surface wave forcing, and the second and the third term represent the flow driven by wind and barotropic tides, respectively.

#### 2.4. Particle Tracking

Residence time was estimated to determine how flow affects the retention of water across the reef and consequently how that relates to various physical and biological features on the reef flat. A quasi-Lagrangian framework, similar to DeCarlo, Cohen, Wong, Shiah, et al. (2017), was used to determine the residence time ( $T_{RT}$ ) of a water particle on the reef flat. Using water velocity, pressure, and bathymetry data, water particles were tracked from discrete locations across the reef flat. The residence time was estimated using depth-averaged velocity (in two-dimensions) and water depth ( $h(x,t)$ ) at E3 and E5 (Figure 1), and Light Detection and Ranging based bathymetry data (resolution = 3 m, Shih et al., 2011) for the reef flat. Velocities across the reef were estimated by linearly interpolating the transport (Equation 1) between E3 and E5 when the particle was between the two stations, and applying transport at E3 from the reef crest to E3 and applying transport at E5 from E5 to the lagoon boundary. The tidal difference ( $\eta_0$ ) in water depth for each time step was interpolated in the same way, and the water depth relative to mean sea level ( $h$ ) at each location was used to calculate total depth at any location across the reef flat ( $D = \eta_0 + h$ ). Velocity was not measured at any alongshore locations, so transport on the measured cross section was applied to the north and south in the region that bathymetry data was available ( $\sim 1,500$  m to the north,  $\sim 2,000$  m to the south of the cross section). The assumption that transport does not vary in the along reef direction is reasonable for an elongated reef (length  $\gg$  width) where bathymetry does not vary substantially and waves break uniformly along the length of the reef. If the particle reached the north/south boundary, particle tracking was stopped.

Residence time ( $T_{RT}$ ) was calculated in two different ways to determine: (1) where the water at different locations on the reef is coming from, and (2) to determine the effect of varying depth and flow direction on residence time. First, residence time was calculated backward in time from discrete locations across the reef flat to the reef crest or lagoon boundaries to determine where water across the reef flat is coming from. Water particles were tracked across the reef flat until they reach the reef crest or lagoon boundary of the reef flat, as defined in Figures 1c and 1d. Second, particles were started at the reef crest and tracked forward in time to determine the time it takes for water to move across the reef flat with constant (averaged) and actual depth and transport values.

### 3. Results

#### 3.1. Oceanographic Conditions

Conditions at the start of the deployment (approximately 4–7 June) were calm, with low wind and waves. Tropical Storm Hagibis formed in the northern SCS around 12 June and led to higher wind and wave conditions at the atoll.

Measurements from the meteorological station located on Pratas Island (Figure 1b) showed that wind (Figure 2a) near the start of the deployment, 4–7 June, was on average  $1.9 \text{ m s}^{-1}$  toward the northeast, and increased from 7 to 10 June, average of  $2.9 \text{ m s}^{-1}$  with gusts up to  $11 \text{ m s}^{-1}$ . From 10 to 14 June, the wind changed direction toward the southwest, and was on average  $3.0 \text{ m s}^{-1}$ . The highest wind was seen on 14–16 June, on average  $5.7 \text{ m s}^{-1}$  toward the southeast and then northeast, with peak wind up to  $17 \text{ m s}^{-1}$ .

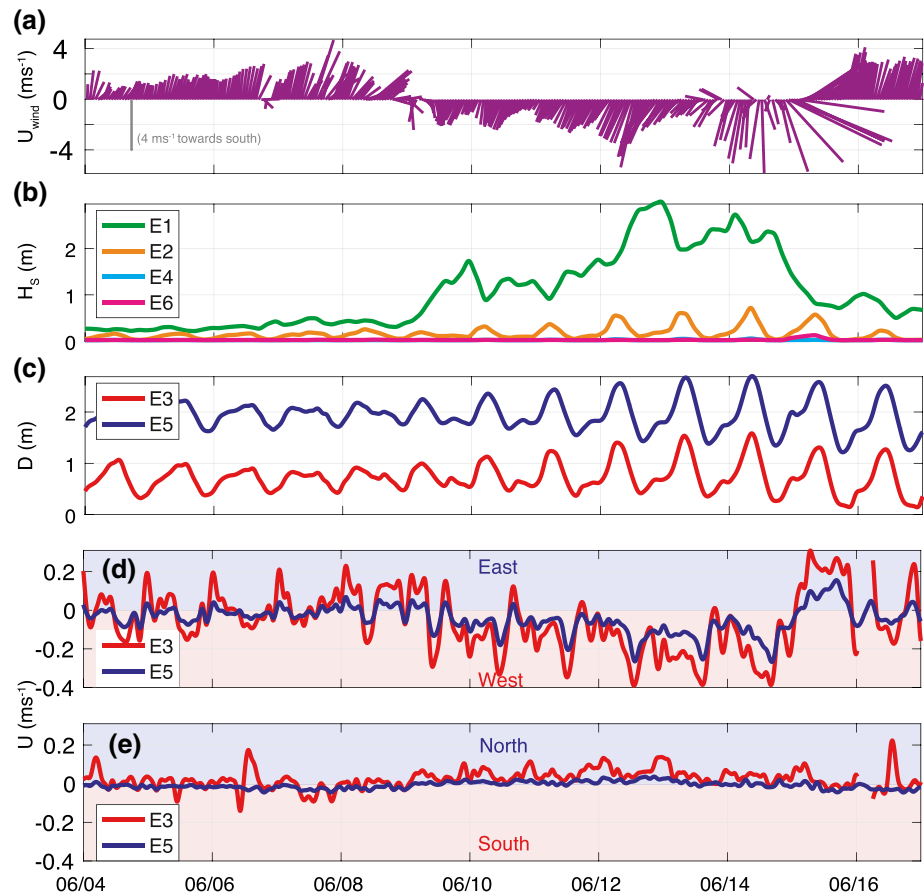


**Figure 2.** Oceanographic conditions during deployment. Panel (a) Wind magnitude and direction (N-S, y axis; E-W, x axis) stick plot with vertical gray bar indicating a magnitude of  $4 \text{ ms}^{-1}$  toward the south. Panel (b) Significant wave height  $H_s$  at E1, E2, E4, and E6. Panel (c) Water depth at E3 and E5. Panel (d) Depth-averaged cross-shore (positive = eastward) and panel (e) along-shore (positive = northward) currents, at E3 and E5. Observational data in all panels are 3 h low pass filtered.

Significant wave height,  $H_s$ , (Figure 2b), measured offshore of the reef crest at E1, (Figure 1c), ranged from 0.2 to 3.0 m, with a period of smaller waves from 4 to 8 June and larger waves from 9 to 15 June. Offshore waves, measured at E1, break on the reef crest, dissipating most of their energy and contributing to setup and creating a pressure driven flow over the reef flat. However, some of the offshore wave energy is transferred onto the reef flat, as seen in the wave signal at E2 to E6. Wave height measured at E2 was significantly lower than at E1, ranging from 0 to 0.7 m, and was modulated by the tide. Waves at E4 and E6 are near zero throughout the deployment, however, on 15 June wave height at E6 increases to 0.1 m, associated with high tide, strong wind toward the northeast and waves coming from the lagoon.

Spring tides occurred on 29 May (before the deployment began) and June 13, 2014. The daily tidal range during the deployment was between 0.4 and 1.3 m at E3, and between 0.4 and 1.4 m at E5 (Figure 2c).

Currents on the reef flat were primarily directed in the cross-reef direction throughout the deployment. Average magnitude of the cross-shore currents was  $0.14 \text{ m s}^{-1}$  at E3 and  $0.06 \text{ m s}^{-1}$  at E5 from 4 to 17 June. The average magnitude of cross reef transport is  $0.11 \text{ m}^2 \text{ s}^{-1}$  and  $0.12 \text{ m}^2 \text{ s}^{-1}$  at E3 and E5, respectively. A small increase in transport at E5 is expected due to the annular shape of the atoll. Average magnitude of the along-shore currents on the reef was  $0.03 \text{ m s}^{-1}$  at E3 and  $0.02 \text{ m s}^{-1}$  at E5 (Figure 2e). At the start of the study (4–8 June), cross-shore currents were slower and tidally reversing, and average cross-shore current magnitudes were  $0.07 \text{ m s}^{-1}$  at E3 and  $0.03 \text{ m s}^{-1}$  at E5 (Figure 2d). On 8–15 June, currents increased and were primarily in the westward direction (toward the lagoon), with average cross-shore current magnitudes of  $0.16 \text{ m s}^{-1}$  at E3 and  $0.08 \text{ m s}^{-1}$  at E5.

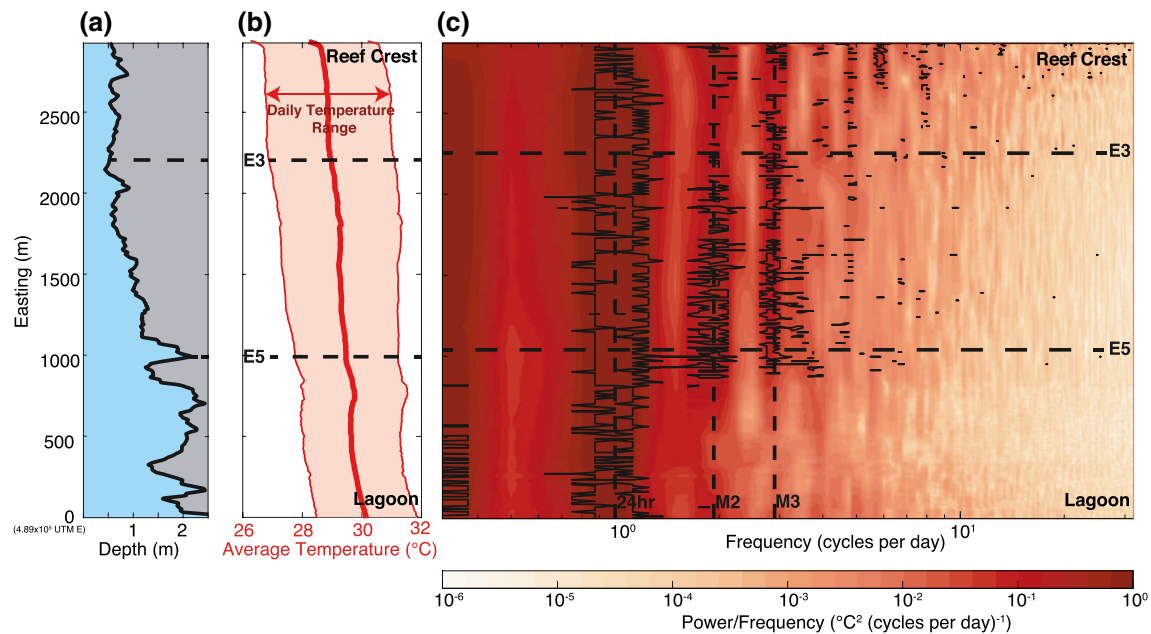


**Figure 3.** Environmental gradients across the east reef flat. Panel (a) Depth below mean sea level associated with each point along the DTS cable. Panel (b) Average near-bottom temperature from the DTS data across the east reef flat in red. Average DTR across the east reef flat shown as the shaded area ( $\pm 0.5$  DTR from the mean temperature). Panel (c) Power spectral density of near-bottom temperature across the east reef flat from the DTS data. Statistically significant peaks in the spectral analysis are outlined in black. The dashed black lines denote the diurnal (24 h), semidiurnal (M2 tidal component) and terdiurnal (M3 tidal component) frequencies. All DTS data are averaged in 10 m sections. DTR, Daily temperature range; DTS, Distributed Temperature Sensing.

### 3.2. Variability in Temperature Across the Reef

The high spatial resolution of water temperature available from the DTS data allows us to examine near-bed thermal environments across the reef. Mean temperature over the study period (Figure 3b) is highest near the lagoon ( $\sim 30.0^{\circ}\text{C}$ ), and lowest at the reef crest ( $\sim 28.5^{\circ}\text{C}$ ) where cool offshore water is brought onshore. Large internal waves shoaling on the east foreereef of Dongsha Atoll bring cold, nutrient-rich water to the near surface, which is then transported westward onto the reef flat by tides, wind, and surface waves (Reid et al., 2019). Daily intrusions of cool offshore water are seen in the DTS observations, when currents are directed in the onshore (westward) direction (see Figure 2 in Reid et al., 2019).

Daily temperature range (DTR) has been shown to be an influential metric for characterizing high-frequency temperature variability on coral reefs and thermal resilience (Safaie et al., 2018). DTR varies across the reef, ranging from approximately  $4.2^{\circ}\text{C}$  near the reef crest, where water depth is shallower, to  $3.1^{\circ}\text{C}$  near the lagoon, the deepest part the reef flat (Figures 3a and 3b).

From the spectral analysis (Figure 3c), it is evident that there is significant diurnal variation in water temperature across the entire reef flat. This is likely due to daily heating and cooling from solar insolation of water on the shallow reef and the diurnal component of the tidal flow. Additionally, there are significant peaks at the M2 and M3 tidal frequencies near the middle of the reef flat and toward the reef crest, corresponding to similar spectral peaks in the pressure data which are likely due to the semi-diurnal and higher frequency tidal harmonics present on the shallow reef flat. There is also significant higher frequency variability ( $>3$  cpd) close to the reef crest.

### 3.3. Physical Processes Driving Circulation on the Reef Flat

Reid et al. (2019) completed a heat budget analysis for the Dongsha reef flat, and found that the balance of atmospheric heating and advection of heat across the reef accurately predicts the observed heating rates on the reef flat. The contribution of atmospheric and advective heat flux varied throughout the deployment at E3 and E5 (see Reid et al., 2019—Figure 2 for a composite day and Figure S1 for 8 days of the heat budget), but on average these terms contributed approximately equally to the rate of change of temperature on the



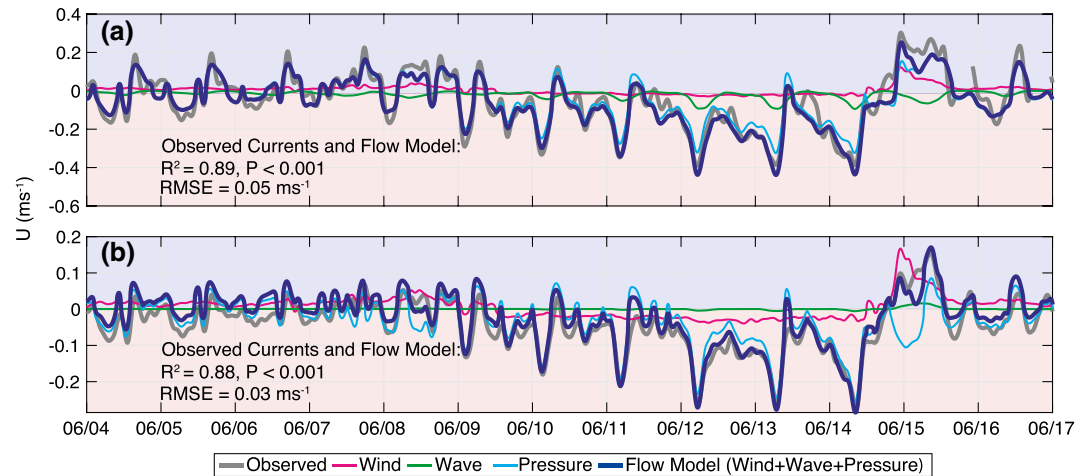


**Figure 4.** Cross-shore flow model. Panel (a) and (b) show the observed currents (gray) and the three components of the flow model: wind (pink), waves (green) and pressure gradient (light blue) for E3 and E5, respectively. The sum of the three components of the flow model is shown in dark blue.

reef flat. Tides, wind, and waves are driving flow across the reef flat, and subsequently contributing to the advection of heat across the reef. Understanding the physical processes which are contributing to the advective heat flux across the reef can explain the patterns of variability seen in the temperature across the reef flat.

The flow predicted using Equation 10 was compared to observed currents on the reef flat at E3 and E5. This simple analytical model (Equation 10) reproduced the observed reef flat currents with a  $R^2$  of 0.89 and 0.88 ( $p < 0.001$ ) at E3 and E5, respectively (Figure 4). The root-mean-squared error between the model and the observed reef flat currents was  $0.05 \text{ m s}^{-1}$  and  $0.03 \text{ m s}^{-1}$  at E3 and E5, respectively.

The terms in Equation 11 were used to attribute flow forcing to waves, wind and tides (described in Section 2.3). For the entire deployment, the wind stress term accounted for on average 2% of the flow at E3. Waves, driven by the wave radiation stress and residual pressure gradients terms, and tidal pressure gradients each accounted for approximately half of the flow at E3. At E5, surface waves and tide account for 42% and 40% of flow, respectively, and wind accounts for 18% flow. Complications and interdependencies between terms in this simple analytical solution are discussed in Section 4.1.

### 3.4. Residence Time

The origin (offshore vs. lagoon) of water flowing onto the reef and the residence time of that water on the reef flat both influence the spatial gradients in mean temperature and DTR seen in Figure 3. Residence time was estimated by tracking water particles backward in time from six starting locations on the reef (Figure 5g, A–F). Only particles that originated from reef crest or the lagoon (as indicated by the dashed lines in Figure 5g) were used for residence time estimates. The average residence time was 3.6 h near the reef crest (Figure 5, location F), and increased to 8.6 h near the lagoon (location A). Particles that end near the reef crest (location F, Figure 5f) have short residence times (0–3 h), with a positively skewed tail toward longer residence times. This distribution holds across the middle of the reef flat (location D to F, Figures 5d–5f) but becomes more evenly spread (i.e., a more normal distribution) toward the lagoon (location A to C, Figures 5a–5c). At locations A to C, the most common residence times are 3–6 h.

During our study period, near the reef crest (location F) 83% of the particles originated from offshore, and only 3% came from the lagoon. Near the lagoon (location A), the percentage of particles that came from offshore decreases to 50%, while the water particles that came from the lagoon increases to 21%. The remainder of particles could not be tracked to one of these boundaries because they traveled alongshore to the north or south.

Residence time varied throughout the deployment, and the source of the water also varied. At the start of the deployment (4–5 June), closer to the spring tide and when wind and waves are small, residence times

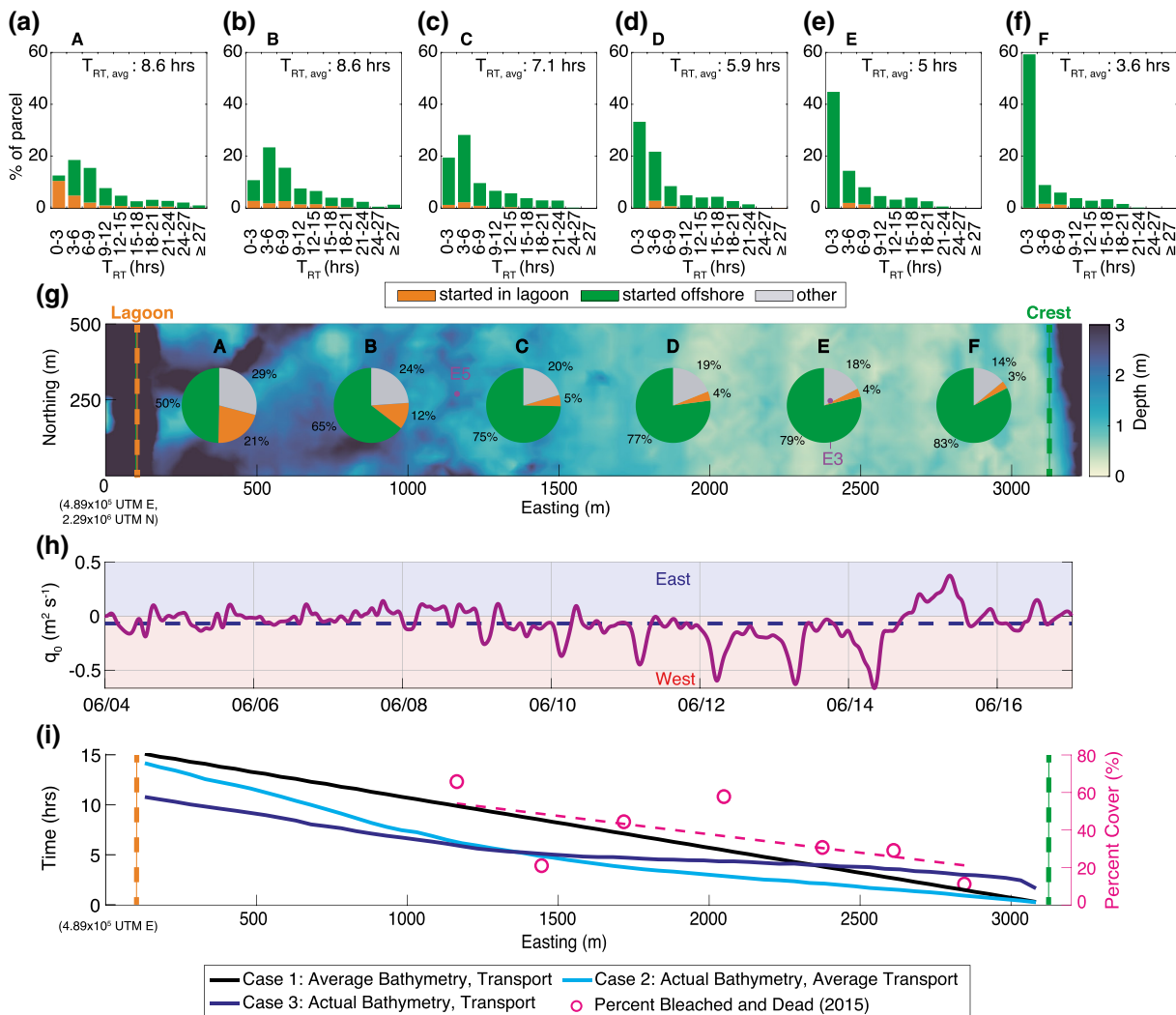


**Figure 5.** Residence time estimates across reef flat. Panels (a) to (f) the percentage of particles that started either from the lagoon or offshore from the locations in Panel (g), and the distribution of residence times. Panel (g) pie charts show at that location on the reef flat the total percentage of particles that started in either the lagoon or offshore. “Other” includes tracks that came from the north/south or insufficient data. Panel (h) Average cross shore transport in blue dashed line (positive = eastward), and actual cross shore transport across the reef flat in purple. Panel (i) the time it takes for a particle started at the reef crest to move across the reef (Section 3.4) for Case 1 shown in black (average bathymetry and transport across the reef flat), Case 2 shown in light blue (actual bathymetry and average transport) and Case 3 shown in dark blue (actual bathymetry and transport). The percent of total coral cover that was bleached or dead after a bleaching event in 2015 (DeCarlo, Cohen, Wong, Davis, et al., 2017) is shown in pink, with a linear fit to the data.

at points C and D (Figure 5g) were on average 11 h. During this time, 94% of the particles are coming from offshore. During the neap tide (6–8 June), residence times were slightly longer (~13 h), however, during this time, 46% of particles were coming from offshore, and 52% are coming from the lagoon (the remainder come from the north/south). Although the residence time was similar when comparing spring and neap, the source of the water changed. When wind and waves picked up (9–13 June), residence times were much shorter (~ 3 h), and 100% of particles were coming from offshore.

In order to understand how depth and variability in current speed and direction affect residence time estimates on the reef flat, the time for a particle starting at the reef crest to move across the reef flat was determined. Particles are tracked forward in time in three different ways: (1) using an average onshore (westward) transport (Figure 5h) and average depth (1.23 m) across the entire reef flat, (2) using an average onshore (westward) transport and actual depth across the reef flat, and (3) using actual transport and depth across the reef flat.

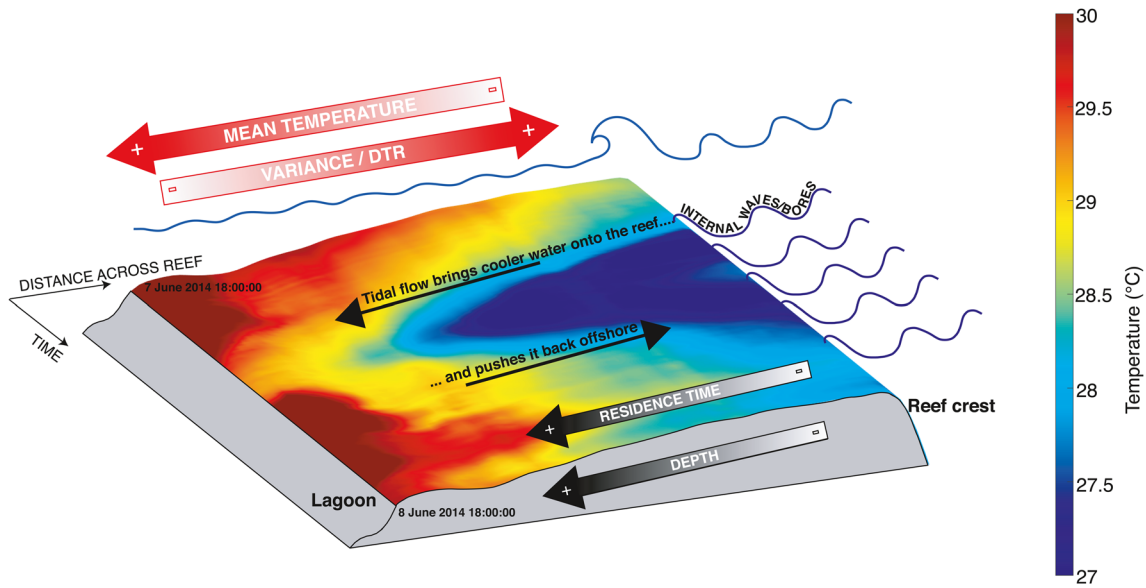


**Figure 6.** Example of DTS data for 7–8 June 2014. A quasi-3D view of continuous near-bed temperature measurements across a 3-km cross section of the east reef flat. Bathymetry is smoothed for the cross section of the reef where the DTS is located. DTS, Distributed Temperature Sensing.

Case 1 is the simplest way to think of transit time of a particle from the reef crest to lagoon, and predicts shorter residence times near the offshore (eastern) edge of the reef, and longer times further onshore toward the lagoon (black line, Figure 5i). Variability in the depth of water across the reef flat can have a significant impact on the residence time of water (Case 2, light blue, Figure 5i). For Dongsha, the actual bathymetry decreases the time it takes for a particle to move across the reef flat, because residence times are significantly shorter in the first half of the reef flat where depths are shallower than the average (Case 1). The time it takes for a particle to move across the first half (~1,500 m) of the reef flat is approximately 5 h, which is shorter than case 1 (~8 h). As depth increases toward the lagoon, the slope of the line increases as particles slow down in deeper water (Figure 5i), and residence times for case 1 and 2 converge near the lagoon.

Variability in the current speed and direction also leads to complex patterns of residence time across the reef. Tidal fluctuations in flow direction (Case 3, dark blue, Figure 5i) lead to longer residence times closer to the reef crest, because currents are not always directed onshore (westward). In the back half of the reef particles slow down in deeper water, similar to case 2, however the time to reach the back of the reef (~11 h) is shorter than Case 1 and 2 (~15 h), because the observed transport was greater and primarily directed toward the lagoon during the second half of the deployment when wind and waves increased.

## 4. Discussion

The reef flat at Dongsha Atoll is anomalously wide (~3 km), compared to other reefs in the literature (Falter et al., 2013; Goldberg, 2016), and this contributes to the observed patterns of flow and spatial temperature variability (Figure 6; also see Figure 2 in Reid et al., 2019, for 8 days of DTS data). Our measurements indicate that flow on the reef flat is driven primarily by tides, wind, and surface waves (Section 3.3). These physical processes govern the residence time of water across the reef flat, creating gradients in mean temperature, DTR and likely other chemical parameters, although these were not measured.

### 4.1. Physical Processes on a Wide Reef Flat

In Section 3.3, Equation 11 is used to separate the physical forcings driving flow across the reef flat due to surface gravity waves, tides, and wind stress. The short duration of our field experiment and inherent interdependence in these forces introduce complications to this simple attribution, which we will discuss further in this section.

The pressure gradient term (the last term under the radical in Equation 10) represents reef-scale pressure gradients due to tides, wind, and surface gravity wave setup. As discussed in Section 2.3, surface tides contribute significantly to the pressure gradient term, accounting for 38% and 32% of the variability of  $\Delta\eta$  at E3 and E5, respectively. The remainder of the pressure gradient term ( $\Delta\eta_r$ ) was attributed to pressure driven flow from sea level setup by surface gravity waves breaking on the reef crest. From 9 to 15 June significant wave height at E1 is large ( $>1$  m, Figure 2b), and during this period, there is a large, low frequency pressure gradient at both E3 and E5 due to offshore wave setup (Figure 4). The tidal residual pressure gradient ( $\Delta\eta_r = \Delta\eta - \Delta\eta_{\text{tide}}$ ) was compared to offshore wave height at E1. The residual pressure gradient term ( $\Delta\eta_r$ ) was significantly correlated with offshore wave height at E3 and E5,  $R^2 = 0.65$  and  $0.43$ ,  $p < 0.0001$ , respectively. This correlation indicates that waves are driving sea surface elevation change, and consequently flow on the reef flat, even as far back on the reef as E5.

The two-week duration of our observations does not permit the resolution and prediction of all tidal constituents, and thus the residual pressure gradient term ( $\Delta\eta_r$ ) likely still includes some influence from tides. Additionally, the tidal response of the lagoon lags the ocean by approximately 40 min—appearing as a pressure gradient between the open ocean and the lagoon. This is also imperfectly captured by our tidal analysis. Tidal modulation of wave radiation stress at the reef crest (e.g., Becker et al., 2014) can be clearly seen in the tidal variations in significant wave heights at E2 relative to the offshore wave heights at E1 (Figure 2b). If tidally modulated wave radiation stress dominated the tidal component of the pressure gradient term ( $\Delta\eta_{\text{tide}}$ ), we would expect it to peak at low tide; however,  $\Delta\eta_{\text{tide}}$  exhibits a  $90^\circ$  phase difference with the sea level at E3, consistent with tidal forcing.

Previous observations on reefs flats, often with narrower widths than Dongsha, have shown that wind is almost never a dominant force and flow is instead driven primarily by a pressure gradient from surface wave setup or tidal driven flow (Hench et al., 2008; Rogers et al., 2016; Taebi et al., 2011). The average contribution of wind driven flow from 4 to 14 June was 2% and 17% at E3 and E5, respectively. The contribution of wind driven flow increased to 9% and 37% at E3 and E5, respectively, on 15 June, when wind toward the northeast greatly increased. During this windy period, the contribution of the wind stress term at E5 is greater than the wave and tidal forcing.

Wind-driven sea level changes in the lagoon could also be contributing to the pressure gradient driving flow across the reef flat. The wind stress term (in Equation 11) only takes into account local wind stress at that location on the reef. For example, an eastward wind, like that which occurred on 15 June, may cause sea level to rise on the east side of the lagoon (on the west side of the reef flat) contributing to pressure driven flow on the reef flat. And, as expected, on 15 June, the strong eastward wind event is accompanied by coincident increase in both the wind stress and the pressure gradient term driving flow across the reef flat. However, on average, the magnitude of the wind was not significantly correlated with the residual pressure gradient term ( $\Delta\eta_r$ ) during our study period.

The internal tide at Dongsha Atoll influences the sea surface height offshore of the reef crest, and subsequently the pressure gradient which is driving flow across the reef flat. The residual between the sea surface height measured offshore of the reef crest at E1 ( $\eta_{E1}$ ) and the barotropic tidal sea level variation ( $\eta_{\text{tide}}$ ), estimated using the OTIS model and TMD toolbox (Egbert & Erofeeva, 2002; Padman & Erofeeva, 2004), was bandpass filtered (10–26 h) and used to estimate the sea level variation due to the internal tide at E1 ( $\eta_{\text{IT}}$ ). The standard deviation of  $\eta_{\text{IT}}$  was 20% of that for  $\eta_{\text{tide}}$  on the forereef; however, the spatial gradient in sea level across the reef flat ( $\Delta\eta_{\text{IT}}$ ) may be significant, since  $\eta_{\text{IT}}$  in the lagoon is likely near zero. This offshore sea level variation due to internal tides is small compared to the barotropic tide, but it may play a significant role in driving flow over the reef flat.

Barotropic tides have a significant effect on flow across the reef flat, accounting for 48% and 41% of the flow variance at E3 and E5, respectively. On the wide reef flat, the tidal excursion, or the distance that a water particle moves over one tidal cycle, varies on fortnightly timescales. From the DTS data, it is evident that cooler offshore water comes onshore during the flood tide and sometimes reaches the lagoon (Figure 6; also see Figure 2 in Reid et al., 2019, for 8 days of DTS data). However, on smaller flood tides the cooler offshore water does not make it all the way to the lagoon, but goes back offshore (eastward). For example, on 8 June, during the neap tide and low wave conditions, cold water comes onshore (westward) during the flood, and

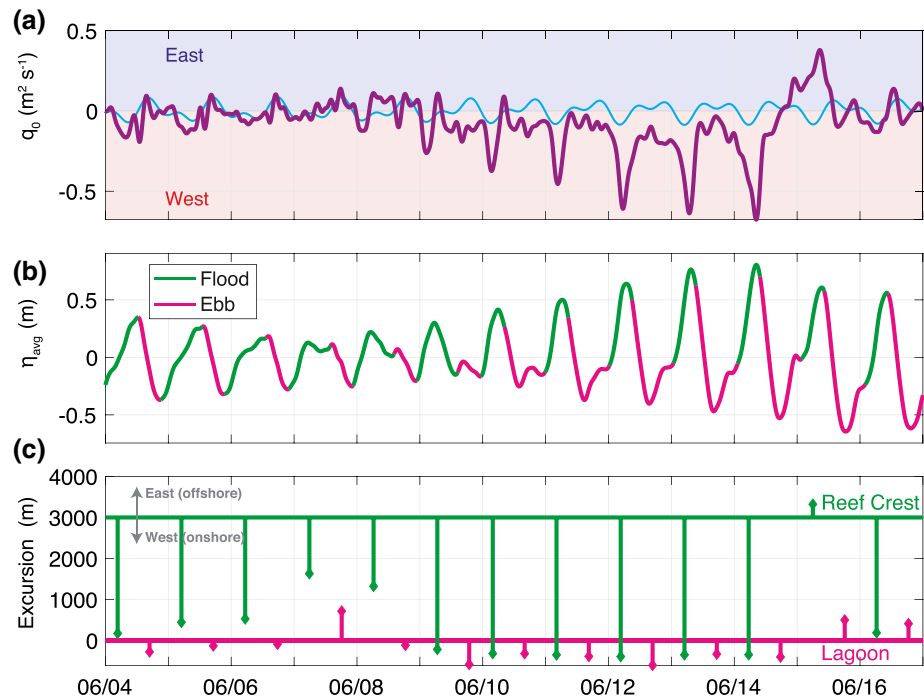


**Figure 7.** Panel (a) Cross-shore transport in purple (positive = eastward), and detrended tidal component of the cross-shore transport in light blue. Panel (b) Average sea level variation across the reef flat, with the flood timing in green and ebb timing in pink. Panel (c) Cross-shore excursion during floods (green) from the reef crest and ebbs (pink) from the lagoon boundary.

when currents turn around (eastward), the cold water goes back offshore (Figure 6). The contribution of tides to flow (Equation 11) on 8 June was on average 38% and 40% at E3 and E5, respectively. On 4 June, when wave conditions were similar to 8 June, stronger tidal currents push cold water all the way across the reef flat (westward) during the flood tide (see Figure 2 in Reid et al., 2019). On 4 June, the contribution of tides to the flow was much greater, 55% and 53% at E3 and E5, respectively.

To understand how tidal excursion of offshore water varies, particles were tracked forward in time from the reef crest at the start of every flood tide to estimate the total cross-shore distance the particle travels during a flood. The time of onshore (flood) and offshore (ebb) transport was determined by looking at the detrended tidal diurnal and semi-diurnal component of the average across-shore transport (Figure 7a). Particles were tracked from the reef crest when tidal currents were directed onshore (westward), for the duration of the flood.

On average, particles traveled approximately 2,570 m (approximately 85% of the reef width) westward toward the lagoon during flood tides (Figure 7c). At the start of the deployment (4–9 June), there were no significant waves or wind driving flow across the reef flat (Figures 2a and 2b), therefore, the flow was largely tidally driven. During the flood tide on 4–5 June, near the end of the spring tide, particles traveled westward from the reef crest on average 2,700 toward the lagoon. On 6–8 June, before wind and waves picked up, particles did not make it into the lagoon, traveling on average 1840 m, during the flood. This is because of weaker currents on the reef flat during the neap tide. On 10–14 June, wind and waves picked up, and particles traveled across the reef flat into the lagoon (>3,000 m). On 15 June, even during the flood tide, high wind toward the northeast pushed water particles at the reef crest offshore (eastward).

Particles were also tracked from the lagoon boundary during the ebb tides to estimate the excursion length during ebb and the influence of lagoon-origin water across the reef flat. During the ebbs on 4–8 June, particles stayed near the lagoon boundary, traveling on average 5 m toward the reef crest, and were also carried alongshore (Figure 7c). When wind and waves pick up on 9–14 June, particles were transported directly into the lagoon during the ebb tide, not entering the reef flat.



There is significant asymmetry in the tidal excursion of water on the reef flat that is evident when tides were primarily driving flow near the start of the deployment (4–8 June). During the flood tides, offshore water is moving on average 2,200 m onshore (westward); however, during the ebb tides, lagoon water is moving on average 5 m onto the reef flat. This results in more offshore water than lagoon water coming onto the reef flat, which could significantly impact the biogeochemistry on the reef flat. Additionally, in our observations, the average tidal excursion length is less than the width of the reef flat, contributing to increased residence time of water on the reef.

#### 4.2. Formation of Environmental Gradients

A heat budget analysis for the Dongsha Atoll reef flat (current study site) by Reid et al. (2019) indicates that atmosphere-ocean surface heat flux and advective heat flux contribute in approximately equal parts to the change in temperature across the reef. In this study, we examine the physical mechanisms contributing to the advective flux of water on the reef flat and find that surface waves, tides, and wind were all important during our study period. These physical mechanisms combined with variable water depth on the reef flat can create complex patterns in the residence time of water on the reef and correspondingly, environmental gradients in temperature (Figure 6).

Daily temperature range (Section 3.2) was highest ( $\sim 4.3^{\circ}\text{C}$ ), and mean temperatures were lowest ( $\sim 29.0^{\circ}\text{C}$ ) near the reef crest. The high DTR near the reef crest and E3 is not only due to daily heating and cooling (surface heat flux) on the shallow reef flat, but also due to high frequency variability in offshore source water and time-variable, tidally forced advective heat flux. Seawater offshore of the reef crest is often cold and highly variable in temperature due to deep water mixed to the surface by shoaling internal waves (Davis et al., 2020). This water is subsequently forced onto the reef flat by tides, wind and waves (see Reid et al., 2019), contributing to the low mean temperature and high variability observed near the reef crest (Figure 3). The shallow water depths near the reef crest lead to strong currents and short residence times (Section 3.4).

The DTR is lowest ( $\sim 3.2^{\circ}\text{C}$ ), and mean temperatures are highest ( $\sim 30.0^{\circ}\text{C}$ ) further back on the reef flat near the lagoon. Here, the water is deeper, and has longer residence times. This stagnant water can heat up during the day, contributing to a peak in the temperature spectrum at one cycle per day (Figure 3) and is subject to less variability in temperature. Also, there is less of an influence of offshore cool water here, leading to higher mean temperatures.

In the Red Sea, Davis et al. (2011) and Pineda et al. (2013) showed that wave-protected regions on the back of the reef flat had highest mean temperatures, and wave-exposed regions near the reef crest had lower mean temperatures, consistent with observations on Dongsha Atoll. However, these studies also found that the wave-protected regions of the reef flat had the greatest temperature variability—unlike our findings on Dongsha Atoll. On the Red Sea reefs, regions with low temperature variability were located near the reef crest where surface wave forcing was strong, but there were no internal waves. On the east reef flat at Dongsha, we see the opposite spatial pattern in temperature variability, with the surface and internal wave-exposed reef crest having the highest temperature variability. Davis et al. (2011) and Cyronak et al. (2020) also find that shallow regions have the highest temperature variability, consistent with our observations on Dongsha Atoll.

#### 4.3. Patterns in Benthic Cover and Bleaching

Thermal tolerance of corals has been shown to vary substantially within an individual reef (e.g., Pineda et al., 2013; Palumbi et al., 2014; Safaie et al., 2018), and studies suggest that reefs that normally experience a variable thermal environment may have a higher temperature tolerance (McClanahan et al., 2005; Oliver & Palumbi, 2011; Palumbi et al., 2014; Safaie et al., 2018). The physical mechanisms driving flow, and resulting residence times across the reef flat are connected to the physical environment and biogeochemistry, and consequently can affect community structure and thermal tolerance of coral reefs. While the physical forcings on the reef flat, primarily tidal and surface waves, and resultant residence times presented here are specific to our two week deployment, we expect that these patterns would be similar outside of our observational period. These results may give some insight into the patterns of benthic cover and bleaching seen at Dongsha Atoll.

In 2015, an ecological survey of the Dongsha Atoll reef flat (current study site) was conducted to quantify coral genera and substrate type both before and after a coral bleaching event (Figure 5i; DeCarlo, Cohen, Wong, Davis, et al., 2017). The eastern region of the reef flat, near the reef crest, which had shorter residence times and higher temperature variability during our deployment, had a smaller percentage of corals that bleached or died (Figure 5i). This is in contrast to a study by McClanahan et al. (2005) in Mauritius, where they saw that regions with high water flow, that were typically further offshore, experienced higher bleaching intensity. Mean temperature and residence time are both lowest at the reef crest and increase toward the back of the reef (Figure 6). On Dongsha Atoll, during this deployment, temperature variability and residence time have an inverse relationship, with short residence times being associated with high variability and long residence times with low variability.

At our study site, DeCarlo, Cohen, Wong, Shiah, et al. (2017) found relatively low coral cover (6%) near the reef crest, likely due to mechanical breakage from large offshore surface waves breaking on the reef crest (Section 3.3). From E3 to E5 coral cover was fairly consistent, at an average 27%, while toward the lagoon side of the reef flat the benthic cover shifts to almost entirely seagrass (78% cover), with very little coral cover (DeCarlo, Cohen, Wong, Shiah, et al., 2017). A study by Rogers et al. (2016) at Palmyra Atoll showed regions with moderate to high coral cover (>10%) had lower mean temperatures than regions with low or no coral cover (<10%). They also observed low coral cover in the back-reef and lagoon, where mean temperatures were higher, and travel times are longer. This trend is consistent with the results seen during this deployment, where the back-reef region (E6) mean temperatures were the highest and there was almost no live coral cover (DeCarlo, Cohen, Wong, Shiah, et al., 2017).

High frequency temperature variability (i.e., DTR) was shown to be the most influential metric in predicting bleaching prevalence on coral reefs in a global study by Safaie et al. (2018). On Ofu Island, in American Samoa, Oliver and Palumbi (2011) also showed that environmental variability across an individual reef can lead to variable bleaching responses. Corals living in more variable environments had increased thermal tolerance, and lower rates of mortality. On Dongsha Atoll from the reef crest to the middle of the reef, E2 to E5, there was significant variability in temperature at higher frequencies during our deployment (>24 h, Figure 3c). A survey by DeCarlo, Cohen, Wong, Davis, et al. (2017) after a severe bleaching event at Dongsha Atoll in 2015 found that the percentage of coral bleached or dead was lowest near the reef crest, and increased further back on the reef flat (Figure 5i).

A study from the Red Sea, documenting reef response to a bleaching event in 2010, showed that bleaching and mortality was most severe on the wave-exposed (offshore) side of the reef platform where mean temperature and variability was lowest (Pineda et al., 2013). The wave-protected (onshore) side of the reef, which has higher mean temperatures, and increased variability, experienced lower mortality. On the Dongsha Atoll reef flat, there are similar patterns in mean temperature (cooler on the offshore/exposed side, warmer on the onshore/protected side), but the opposite pattern in temperature variability seen during this deployment. Pineda et al. (2013) explain the observed pattern in mortality is likely due to previous biological adaptation and acclimatization of corals to high frequency variability, similar to at Ofu (Oliver & Palumbi, 2011). On Dongsha, high temperature variability near the reef crest could lead to low bleaching and mortality in this region.

Safaie et al. (2018) showed that depth was the second most influential metric in predicting bleaching prevalence, with deeper reefs less likely to experience pervasive bleaching. Safaie et al. (2018) note that variability and depth may work in complementary ways to mitigate bleaching, with shallower regions having higher variability and therefore greater thermal tolerance, and deeper regions providing refuge for corals, despite lower variability in temperature. At Dongsha, bleaching and mortality was lowest near the reef crest, where the depth was shallowest and temperature variability was highest (Figures 3 and 5i). Bleaching and mortality increased with depth toward the back of the reef, and variability decreased.

## 5. Conclusion

The observations and analyses presented here show that the processes driving flow on the east reef flat at Dongsha Atoll are tidal pressure gradients, wind stress, and surface waves, and that across the reef flat there is variability in both the residence time of water and the thermal environment.

From a simple analytical model of flow on the reef flat, we find that waves and tides each contributed in approximately equal parts to forcing flow on the eastern part of the reef flat (E3) during our study, and wind only contributed significantly during a large wind event. Further back on the reef toward the lagoon (E5), tides and waves also contributed in equal parts, however wind played a more substantial role in driving flow throughout the deployment, especially during the large wind event. Furthermore, the wide reef flat at Dongsha leads to unique patterns of tidal excursion across the reef flat throughout the deployment.

Residence times across the reef flat are shortest near the reef crest, and increase toward the lagoon. The majority of water near the reef crest is coming from offshore (83%), and only a small portion (3%) comes from the lagoon during this deployment, with the remainder unresolved by our particle tracking model. Closer to the lagoon, approximately half of the water originates from the reef crest (i.e., offshore), and only 21% comes from the lagoon. The source of water can influence the thermal and chemical environment across the reef flat.

Understanding the processes driving flow at different locations on the reef, and the subsequent temperature gradients, can help us to understand the distribution of coral across the reef at Dongsha. This elevated thermal variability is a distinguishing feature of shallow reefs compared to the open ocean, and may influence the thermal tolerance of corals. A better understanding of spatial patterns in thermal microclimates and thermal tolerance can help inform which coral reefs may be more resilient in a changing climate and should be prioritized for protection.

### Data Availability Statement

Data used in this study are available online at Dryad (<https://doi.org/10.7280/D1S38H>).

### Acknowledgments

We are grateful for the support of the Dongsha Atoll Research Station (DARS) and the Dongsha Atoll Marine National Park, whose efforts made this research possible. The authors would also like to thank G. Lohmann from WHOI, G. Wong, L. Hou, F. Shiah, and K. Lee from Academia Sinica for providing logistical and field support. We thank S. Tyler, and J. Selker from the Center for Transformative Environmental Monitoring Programs (CTEMPs), funded by the National Science Foundation (EAR awards 1440596 and 1440506), for timely and effective provision of experimental design support, logistical support and equipment for the project. Support for S. Lentz is from NSF Grant No. OCE-1558343. Support for A. Cohen from NSF Grant No. 1220529, by the Academia Sinica (Taiwan) through a thematic project grant to G. Wong and A. Cohen. Support for E. Reid and K. Davis is from National Science Foundation (NSF) Grant No. OCE-1753317, and support to E. Reid from the Environmental Engineering Henry Samuelli Endowed Fellowship and the UCI Oceans Graduate Fellowship.

### References

- Alford, M. H., Peacock, T., MacKinnon, J. A., Nash, J. D., Buijsman, M. C., Centurioni, L. R., & Tang, T. Y. (2015). The formation and fate of internal waves in the south China Sea. *Nature*, *521*(7550), 65–69.
- Barkley, H. C., Cohen, A. L., Golbuu, Y., Starczak, V. R., DeCarlo, T. M., & Shamberger, K. E. (2015). Changes in coral reef communities across a natural gradient in seawater pH. *Science Advances*, *1*(5), e1500328.
- Becker, B., Merrifield, M., & Ford, M. (2014). Water level effects on breaking wave setup for Pacific island fringing reefs. *Journal of Geophysical Research: Oceans*, *119*(2), 914–932. <https://doi.org/10.1002/2013JC009373>
- Castillo, K. D., Ries, J. B., Weiss, J. M., & Lima, F. P. (2012). Decline of forereef corals in response to recent warming linked to history of thermal exposure. *Nature Climate Change*, *2*(10), 756–760.
- Codiga, D. L. (2011). *Unified tidal analysis and prediction using the UTide Matlab functions*, Narragansett, RI: Graduate School of Oceanography, University of Rhode Island.
- Cyronak, T., Takeshita, Y., Courtney, T. A., DeCarlo, E. H., Eyre, B. D., Kline, D. I., et al. (2020). Diel temperature and pH variability scale with depth across diverse coral reef habitats. *Limnology and Oceanography Letters*, *5*(2), 193–203.
- Dai, C. (2004). Dongsha Atoll in the south China Sea: Past, present and future. In *Islands of the world viii international conference, Kinmen Island, Taiwan*.
- Davis, K. A., Arthur, R. S., Reid, E. C., Rogers, J. S., Fringer, O. B., DeCarlo, T. M., & Cohen, A. L. (2020). Fate of internal waves on a shallow shelf. *Journal of Geophysical Research: Oceans*, *125*(5), <https://doi.org/10.1029/2019JC015377>
- Davis, K. A., Leichter, J. J., Hench, J. L., & Monismith, S. G. (2008). Effects of western boundary current dynamics on the internal wave field of the southeast Florida shelf. *Journal of Geophysical Research*, *113*(C9), <https://doi.org/10.1029/2007JC004699>
- Davis, K. A., Lentz, S. J., Pineda, J., Farrar, J. T., Starczak, V. R., & Churchill, J. H. (2011). Observations of the thermal environment on Red Sea platform reefs: A heat budget analysis. *Coral Reefs*, *30*(S1), 25–36.
- DeCarlo, T. M., Cohen, A. L., Wong, G. T. F., Davis, K. A., Lohmann, P., & Soong, K. (2017). Mass coral mortality under local amplification of 2 degrees C ocean warming. *Scientific Reports*, *7*, 44586. <https://www.nature.com/articles/srep44586>
- DeCarlo, T. M., Cohen, A. L., Wong, G. T. F., Shiah, F., Lentz, S. J., Davis, K. A., & Lohmann, P. (2017). Community production modulates coral reef pH and the sensitivity of ecosystem calcification to ocean acidification. *Journal of Geophysical Research: Oceans*, *122*(1), 745–761. <https://doi.org/10.1002/2016JC012326>
- Donner, S. D. (2009). Coping with commitment: Projected thermal stress on coral reefs under different future scenarios. *PLoS One*, *4*(6), e5712.
- Egbert, G. D., & Erofeeva, S. Y. (2002). Efficient inverse modeling of barotropic ocean tides. *Journal of Atmospheric and Oceanic Technology*, *19*(2), 183–204.
- Falter, J. L., Lowe, R. J., Zhang, Z., & McCulloch, M. (2013). Physical and biological controls on the carbonate chemistry of coral reef waters: Effects of metabolism, wave forcing, sea level, and geomorphology. *PLoS One*, *8*(1), e53303.
- Fu, K.-H., Wang, Y.-H., Laurent, L. S., Simmons, H., & Wang, D.-P. (2012). Shoaling of large-amplitude nonlinear internal waves at Dongsha Atoll in the northern South China Sea. *Continental Shelf Research*, *37*, 1–7.
- Goldberg, W. M. (2016). Atolls of the world: Revisiting the original checklist. *Atoll Research Bulletin*, *610*.
- Gourlay, M. R., & Colleter, G. (2005). Wave-generated flow on coral reefs—An analysis for two-dimensional horizontal reef-tops with steep faces. *Coastal Engineering*, *52*(4), 353–387.

- Guadayol, Silbiger, N. J., Donahue, M. J., & Thomas, F. I. (2014). Patterns in temporal variability of temperature, oxygen and pH along an environmental gradient in a coral reef. *PLoS One*, *9*(1), e85213.
- Hausner, M. B., Suarez, F., Glander, K. E., van de Giesen, N., Selker, J. S., & Tyler, S. W. (2011). Calibrating single-ended fiber-optic Raman spectra distributed temperature sensing data. *Sensors*, *11*(11), 10859–10879.
- Hearn, C. J. (1999). Wave-breaking hydrodynamics within coral reef systems and the effect of changing relative sea level. *Journal of Geophysical Research*, *104*(C12), 30007–30019.
- Hench, J. L., Leichter, J. J., & Monismith, S. G. (2008). Episodic circulation and exchange in a wave-driven coral reef and lagoon system. *Limnology and Oceanography*, *53*(6), 2681–2694.
- Hoegh-Guldberg, O., Mumby, P. J., Hooten, A. J., Steneck, R. S., Greenfield, P., Gomez, E., & Hatziolos, M. E. (2007). Coral reefs under rapid climate change and ocean acidification. *Science*, *318*(5857), 1737–1742.
- Hu, J., Kawamura, H., Hong, H., & Qi, Y. (2000). A review on the currents in the south China Sea: Seasonal circulation, South China Sea warm current and kuroshio intrusion. *Journal of Oceanography*, *56*(6), 607–624.
- Kraines, S., Yanagi, T., Isobe, M., & Komiyama, H. (1998). Wind-wave driven circulation on the coral reef at bora bay, miyako island. *Coral Reefs*, *17*(2), 133–143.
- Leichter, J. J., Helmuth, B., & Fischer, A. M. (2006). Variation beneath the surface: Quantifying complex thermal environments on coral reefs in the caribbean, Bahamas and Florida. *Journal of Marine Research*, *64*(4), 563–588.
- Lentz, S. J., Churchill, J. H., Davis, K. A., Farrar, J. T., Pineda, J., & Starczak, V. (2016). The characteristics and dynamics of wave-driven flow across a platform coral reef in the red sea. *Journal of Geophysical Research: Oceans*, *121*(2), 1360–1376. <https://doi.org/10.1002/2015JC011141>
- Lentz, S. J., Davis, K. A., Churchill, J. H., & DeCarlo, T. M. (2017). Coral reef drag coefficients-water depth dependence. *Journal of Physical Oceanography*, *47*(5), 1061–1075.
- Lilly, J. (2019). *JLab: A data analysis package for matlab*, v. 1.6.6. <http://www.jmlilly.net/software>
- Longuet-Higgins, M. S., & Stewart, R. (1962). Radiation stress and mass transport in gravity waves, with application to 'surf beats'. *Journal of Fluid Mechanics*, *13*(4), 481–504.
- Longuet-Higgins, M. S., & Stewart, R. (1964). Radiation stresses in water waves; a physical discussion, with applications. In *Deep sea research and oceanographic abstracts* (Vol. 11, pp. 529–562). Elsevier. [https://doi.org/10.1016/0011-7471\(64\)90001-4](https://doi.org/10.1016/0011-7471(64)90001-4)
- Lowe, R. J., & Falter, J. L. (2015). Oceanic forcing of coral reefs. *Annual Review of Marine Science*, *7*, 43–66.
- Lowe, R. J., Falter, J. L., Bandet, M. D., Pawlak, G., Atkinson, M. J., Monismith, S. G., & Koseff, J. R. (2005). Spectral wave dissipation over a barrier reef. *Journal of Geophysical Research*, *110*(C4). <https://doi.org/10.1029/2004JC002711>
- Lowe, R. J., Falter, J. L., Monismith, S. G., & Atkinson, M. J. (2009a). A numerical study of circulation in a coastal reef-lagoon system. *Journal of Geophysical Research*, *114*(C6). <https://doi.org/10.1029/2008JC005081>
- Lowe, R. J., Falter, J. L., Monismith, S. G., & Atkinson, M. J. (2009b). Wave-driven circulation of a coastal reef-lagoon system. *Journal of Physical Oceanography*, *39*(4), 873–893. <https://doi.org/10.1175/2008JPO3958.1>
- McClanahan, T., Maina, J., Moothien-Pillay, R., & Baker, A. (2005). Effects of geography, taxa, water flow, and temperature variation on coral bleaching intensity in Mauritius. *Marine Ecology Progress Series*, *298*, 131–142.
- Mei, C. C. (1989). *The applied dynamics of ocean surface waves* (Vol. 1, Singapore, Singapore; River Edge, NJ: World Scientific Publishing Co. Pte Ltd.
- Monismith, S. G. (2007). Hydrodynamics of coral reefs. *Annual Review of Fluid Mechanics*, *39*(1), 37–55.
- Morton, B., & Blackmore, G. (2001). South China Sea. *Marine Pollution Bulletin*, *42*(12), 1236–1263.
- Oliver, T. A., & Palumbi, S. R. (2011). Do fluctuating temperature environments elevate coral thermal tolerance?. *Coral Reefs*, *30*(2), 429–440.
- Padman, L., & Erofeeva, S. (2004). A barotropic inverse tidal model for the arctic ocean. *Geophysical Research Letters*, *31*(2). <https://doi.org/10.1029/2003GL019003>
- Palumbi, S. R., Barshis, D. J., Traylor-Knowles, N., & Bay, R. A. (2014). Mechanisms of reef coral resistance to future climate change. *Science*, *344*(6186), 895–898.
- Pandolfi, J. M., Connolly, S. R., Marshall, D. J., & Cohen, A. L. (2011). Projecting coral reef futures under global warming and ocean acidification. *Science*, *333*(6041), 418–422.
- Pineda, J., Starczak, V., Tarrant, A., Blythe, J., Davis, K., Farrar, T., & da Silva, J. C. (2013). Two spatial scales in a bleaching event: Corals from the mildest and the most extreme thermal environments escape mortality. *Limnology and Oceanography*, *58*(5), 1531–1545.
- Reid, E. C., DeCarlo, T. M., Cohen, A. L., Wong, G. T., Lentz, S. J., Safaie, A., & Davis, K. A. (2019). Internal waves influence the thermal and nutrient environment on a shallow coral reef. *Limnology and Oceanography*, *64*(5), 1949–1965.
- Riegl, B., & Piller, W. E. (2003). Possible refugia for reefs in times of environmental stress. *International Journal of Earth Sciences*, *92*(4), 520–531.
- Rogers, J. S., Monismith, S. G., Koweek, D. A., Torres, W. I., & Dunbar, R. B. (2016). Thermodynamics and hydrodynamics in an atoll reef system and their influence on coral cover. *Limnology and Oceanography*, *61*(6), 2191–2206.
- Rosman, J. H., & Hench, J. L. (2011). A framework for understanding drag parameterizations for coral reefs. *Journal of Geophysical Research*, *116*(C8). <https://doi.org/10.1029/2010JC006892>
- Safaie, A., Silbiger, N. J., McClanahan, T. R., Pawlak, G., Barshis, D. J., Hench, J. L., & Davis, K. A. (2018). High frequency temperature variability reduces the risk of coral bleaching. *Nature Communications*, *9*, 1–12.
- Schramek, T., Colin, P., Merrifield, M., & Terrill, E. (2018). Depth-dependent thermal stress around corals in the tropical pacific ocean. *Geophysical Research Letters*, *45*(18), 9739–9747. <https://doi.org/10.1029/2018GL078782>
- Selker, J. S., Thevenaz, L., Huwald, H., Mallet, A., Luxemburg, W., van de Giesen, N., & Parlange, M. B. (2006). Distributed fiber-optic temperature sensing for hydrologic systems. *Water Resources Research*, *42*(12), 1–8. <https://doi.org/10.1029/2006WR005326>
- Shamberger, K. E., Cohen, A. L., Golbuu, Y., McCorkle, D. C., Lentz, S. J., & Barkley, H. C. (2014). Diverse coral communities in naturally acidified waters of a western pacific reef. *Geophysical Research Letters*, *41*(2), 499–504. <https://doi.org/10.1002/2013GL058489>
- Shih, P. T.-Y., Arumugam, D., & Shyue, S.-W. (2011). Bathymetric lidar survey of penghu islands and dongsha atoll using an ellipsoidal height system for bathymetric mapping in shallow waters and difficult-to-navigate environments. *Sea Technology*, *52*(11), 42–45.
- Sinnett, G., Davis, K. A., Lucas, A. J., Giddings, S. N., Reid, E. C., Harvey, M., & Stokes, I. (2020). Distributed temperature sensing for oceanographic applications. *Journal of Atmospheric and Oceanic Technology*, *37*(11), 1987–1997.
- Symonds, G., Black, K. P., & Young, I. R. (1995). Wave-driven flow over shallow reefs. *Journal of Geophysical Research*, *100*(C2), 2639–2648.
- Taebi, S., Lowe, R. J., Pattiaratchi, C. B., Ivey, G. N., Symonds, G., & Brinkman, R. (2011). Nearshore circulation in a tropical fringing reef system. *Journal of Geophysical Research*, *116*(C2). <https://doi.org/10.1029/2010JC006439>

- Thomson, D. J. (1982). Spectrum estimation and harmonic analysis. *Proceedings of the IEEE*, 70(9), 1055–1096.
- Tyler, S. W., Selker, J. S., Hausner, M. B., Hatch, C. E., Torgersen, T., Thodal, C. E., & Schladow, S. G. (2009). Environmental temperature sensing using Raman spectra DTS fiber-optic methods. *Water Resources Research*, 45(4), 1–11. <https://doi.org/10.1029/2008WR007052>
- Van Hooidonk, R., Maynard, J., Tamelander, J., Gove, J., Ahmadi, G., Raymundo, L., & Planes, S. (2016). Local-scale projections of coral reef futures and implications of the paris agreement. *Scientific Reports*, 6, 39666.
- van Woesik, R., Houk, P., Isechal, A. L., Idechong, J. W., Victor, S., & Golbuu, Y. (2012). Climate-change refugia in the sheltered bays of Palau: Analogs of future reefs. *Ecology Evolution*, 2(10), 2474–2484.
- Wang, Y.-H., Dai, C.-F., & Chen, Y.-Y. (2007). Physical and ecological processes of internal waves on an isolated reef ecosystem in the south China Sea. *Geophysical Research Letters*, 34(18). <https://doi.org/10.1029/2007GL030658>